American Journal of Nano Research and Application
2014; 2(6-1): 27-33
Published online December 19, 2014 (http://www.sciencepublishinggroup.com/j/nano)
doi: 10.11648/j.nano.s.2014020601.14

High resolution imaging of a multi-walled carbon nanotube with energy-filtered photoemission electron microscopy

Andreas Neff[1], Olga Naumov[1], Timna-Josua Kühn[2], Nils Weber[2], Michael Merkel[2], Bernd Abel[1], Aron Varga[1], Katrin R. Siefermann[1, *]

[1]Leibniz Institute of Surface Modification (IOM), Chemical Department, Permoser Strasse 15, 04318 Leipzig, Germany
[2]FOCUS GmbH, Neukirchner Strasse 2, 65510 Hünstetten, Germany

Email address:
katrin.siefermann@iom-leipzig.de (K. R. Siefermann)

To cite this article:
Andreas Neff, Olga Naumov, Timna-Josua Kühn, Nils Weber, Michael Merkel, Bernd Abel, Aron Varga, Katrin R. Siefermann. High Resolution Imaging of a Multi-Walled Carbon Nanotube with Energy-Filtered Photoemission Electron Microscopy. *American Journal of Nano Research and Application*. Special Issue: Green Procurement and Mechanism Design. Vol. 2 No. 6-1, 2014, pp. 27-33.
doi: 10.11648/j.nano.s.2014020601.14

Abstract: Photoemission electron microscopy (PEEM) is a powerful and well established tool in surface science. In recent years, PEEM has been increasingly applied to new terrain, such as imaging of complex nano-objects and functional molecular materials, as well as time-resolved experiments. When applying PEEM to such new terrain, information on the mechanisms causing contrast in the PEEM image is particularly valuable. Here, we present a PEEM study on a complex nano-object – an individual multi-walled carbon nanotube (CNT) – to shed light on the origin of PEEM contrast. The presented PEEM images of the nanotube are of unsurpassed resolution and feature intensity variations along the nanotube. Complementary scanning electron microscopy (SEM) and atomic force microscopy (AFM) measurements on the same nanotube reveal topography as the dominant cause for the contrast observed along the nanotube. Energy-filtered PEEM measurements demonstrate that the contrast between nanotube and substrate mainly originates from their different electronic structures. The measurements further demonstrate that energy-filtered PEEM has the potential to image electronic structure variations of complex nano-objects and materials on nanometer length scales.

Keywords: Photoemission Electron Microscopy, PEEM, Carbon Nanotube, CNT, High Resolution Imaging, Contrast Mechanisms

1. Introduction

Photoemission electron microscopy (PEEM) is a widely used type of emission microscopy. It images electrons emitted from a sample upon irradiation with light, typically UV-light, X-rays or lasers. PEEM has proven a powerful tool for the characterization of nanometer-sized materials and the high spatial resolution has led to considerable advances in this field [1-6]. With aberration correction, a spatial resolution of few nanometers may be achieved [7]. Using femtosecond laser pulses as excitation source, it is possible to investigate ultrafast phenomena on a nanometer scale, such as surface plasmon polaritons [8-10] and carrier-dynamics in solids [11]. Even the combination of PEEM with attosecond pulse trains has been realized [12].

Contrast in the PEEM image is the result of an interplay of work function differences, variation in the density of states, photoionization yields, and topography [13]. An additional source of contrast are local distortions of the electric field on the sample, as the sample itself is part of the electron optical system [14-17]. When PEEM is applied to image complex nano-objects on surfaces, the interplay of these various contrast mechanisms complicates interpretation of resulting images. Here, we present a comprehensive study on an individual multi-walled carbon nanotube (CNT) to reveal major contrast mechanisms.

To date, only few PEEM-studies have been performed on complex nano-objects on surfaces – such as carbon nanotubes (CNTs) [18–21] – despite increasing scientific interest in respective materials and their potential for industrial applications [22–24]. Suzuki et al. have investigated the work function difference of individual single-walled carbon nanotubes on a Si line pattern using X-rays as the excitation source [18,19]. Sangwan has employed a UV-PEEM as a tool for probing field effects in CNT-based transistors [20]. Recently, Bao's group has used a

UV-PEEM to study pod-like CNTs encapsulating iron nanoparticles [21]. UPS and XPS studies of carbon nanotubes have been performed by several groups [25–29] providing insights into their valence-band structure. Besides, CNT networks on an insulating SiO2 substrate were imaged with scanning electron microscopy (SEM) to reveal contrast mechanisms for different electron energies [30,31].

In this work, we present a UV-PEEM image of an isolated multi-walled CNT which features an unsurpassed resolution. In particular, intensity variations along the nanotube are clearly resolved. In order to interpret this observation, we performed complementary scanning electron microscopy (SEM) and atomic force microscopy (AFM) experiments on the exact same nanotube. Additionally, we measured a photoelectron spectrum of a single CNT using an imaging energy filter (IEF) installed in the PEEM. Hereby, we show the possibility of obtaining quantitative information about the electronic structure of nanometer scale objects using photoemission electron microscopy.

2. Experimental

Multi-walled CNTs were grown on carbon paper (Toray TGP-H-120) by chemical vapor deposition as described elsewhere [32], with hydrogen, acetylene, ammonia, and argon as the precursor gases. Nickel nanoparticles served as the growth catalyst. As-grown CNTs were removed from the carbon paper substrate by ultrasonication for one hour in ethanol, forming a suspension. The suspension was drop-cast on a polished SiC substrate (6H, 0001-Orientation, MaTecK GmbH, Germany), previously rinsed with distilled water, acetone, and ethanol. The solvent was allowed to evaporate at ambient conditions. The sample was stored in the PEEM vacuum chamber ($p \sim 5\times10^{-9}$ mbar) for five days prior to the PEEM measurements.

PEEM images were obtained with a UV-PEEM (FOCUS GmbH), using an Hg-lamp with a photon spectrum of 4.9-5.2 eV as excitation source. An imaging energy filter (IEF) integrated in the PEEM allowed for acquisition of energy-resolved images. The IEF is a retarding field analyzer that essentially works as a high pass filter for photoelectrons. Energy-filtered measurements were performed in single event counting mode. For all measurements, the extractor voltage was set to 15 kV at a working distance of 1.8 mm from the sample surface.

The sample was further characterized with a scanning electron microscope (Ultra 55, Carl Zeiss SMT) at accelerating voltages of 1–3 kV. The atomic force microscope (Dimension Icon AFM, Bruker) used in this study was operated in tapping mode using a commercial silicon cantilever (k = 26 N/m).

3. Results and Discussion

Fig. 1a) and b) show PEEM images of the sample at two different magnifications. Both images are background and flat field corrected. Fig. 1a) shows an image with a field of view (FoV) of 50 µm (acquisition time = 10 s). The red arrow points towards an isolated CNT. The CNT appears substantially brighter than the underlying SiC substrate. On the left side of Fig. 1a), a large bright structure is visible, which is attributed to debris from the carbon paper used as the CNT growth substrate.

Fig. 1b) shows a PEEM image of the same CNT, as highlighted with a red arrow in Fig. 1a), but obtained with the highest magnification (FoV = 1.3 µm). This image is averaged over 50 exposures of 10 seconds each. Several kinks along the CNT are visible and well resolved in the PEEM image. The thickness of the CNT is not significantly changing over the length of the tube. A Gaussian fit of a line profile perpendicular to the nanotube (yellow line in Fig. 1b) exhibits a FWHM of 38.3 ± 0.4 nm (Fig. 1c).

As the width of the CNT is on the same order as the resolution of the PEEM, it is difficult to determine the exact spatial resolution of this image. However, it is apparent that it is well below 40 nm. For CNTs, this PEEM image is the one with the highest resolution and the most details published to date. The resolution in our measurement is comparable to previously reported resolutions of 25 nm achieved with other samples with the FOCUS IS-PEEM [33,34].

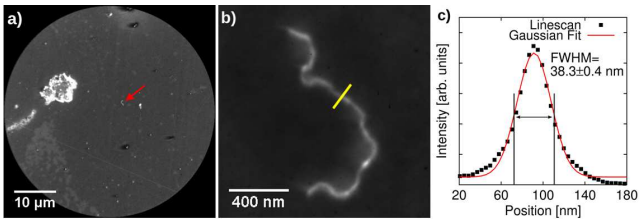

Figure 1. *PEEM measurement showing a) a large field of view (50 µm) image of the sample with an isolated CNT indicated by the red arrow and b) the same CNT at highest magnification. c) Line profile of the intensity along the yellow line in b) together with a Gaussian fit.*

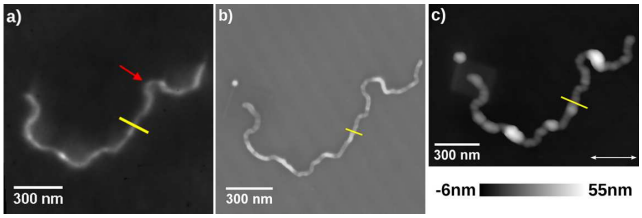

Figure 2. *Comparison of a) PEEM b) SEM and c) AFM measurements of the same CNT. Images a) and b) have been rotated to allow for comparison. The width of the CNT at the indicated positions is 38 nm (PEEM) and 29 nm (SEM), respectively. The arrow in c) indicates the scan direction of the AFM. The height of the CNT in this measurement is 15 nm.*

We attribute the unprecedented resolution and the strong contrast achieved here to two major points: (1) the resolution benefits from the overall flat topography of our sample, as both, the isolated nanotubes and detected debris are without excessive protrusions. We find that the presence of larger CNT agglomerates on the sample is detrimental for the resolution. (2) As we show later, the work function difference between CNTs and the SiC substrate, obtained from the energy-resolved PEEM measurement, exhibits a value as small as 0.35 eV. This is probably small enough to avoid

formation of strong contact potentials, which would lead to increased field distortions, and in general to a lower resolution [14-17].

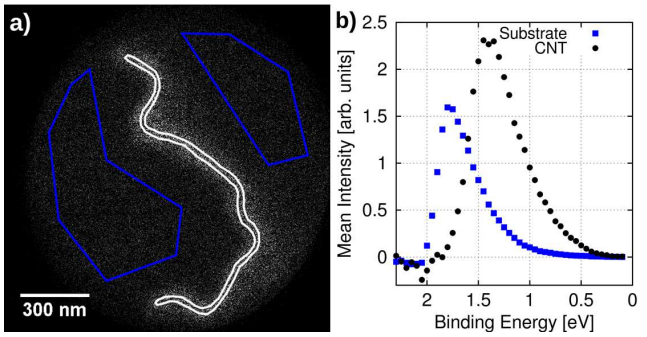

Figure 3. *a) Energy-filtered PEEM image at EB = 1.15 eV. b) Photoelectron spectra of the areas enclosed by the blue lines (SiC substrate) and the white line (CNT) in a).*

The high resolution presented here has not been achieved in respective work by other groups [18–21]. Reasons might be differences in sample preparation, as well as the usage of different combinations of substrate materials and excitation energies.

In order to interpret the variation in intensity along the CNT, we have recorded scanning electron microscopy (SEM) images and atomic force microscopy (AFM) images of the very same CNT previously imaged with PEEM and shown in Fig. 1b). All three images are shown in Fig. 2. The SEM image was obtained at an acceleration voltage of 1 kV and a working distance of 3.8 mm combining the signal of the SE2 (secondary electron detector sideways) and the InLense (secondary electron detector above objective lens) detector at a ratio of 1:1.

The PEEM (Fig. 2a) and SEM (Fig. 2b) images are strikingly similar. This underlines the high resolution achieved in the PEEM image and it indicates that field distortions – which are detrimental for a high resolution PEEM image – are small. The effect of a small field distortion is visible in the loop located in the upper part of the CNT (marked by the arrow). The size of this loop is slightly smaller in the PEEM image compared to the SEM image. The diameter of the CNT determined from the SEM image is 29 nm and thus slightly smaller than the one obtained in the PEEM measurement (FWHM = 38 nm), indicating the better resolution of the SEM. The variation in brightness along the CNT is remarkably similar in the PEEM and SEM image. Bright and dark sections are visible and found to be located at the exact same positions in both images. The origin of this intensity variation is found in the topography of the sample, as evidenced by the AFM image shown in Fig. 2c) and an SEM image obtained at a sample tilt of 30° shown in Fig. S2. Bright spots in the PEEM and SEM image thus correspond to positions at which the CNT is bent up and protruding away from the substrate, leading to local field distortions which in turn result in contrast formation due to change of electron trajectories [14-17,35,36]. We note that the bright spot above the left end of the CNT in Fig. 2b) and c) originates from the SEM measurement, as the electron beam was standing still at that position for a few seconds. As the PEEM measurement was performed before, the spot is not visible in Fig. 2a).

In summary, the PEEM image has an unsurpassed resolution comparable to the respective SEM image. Intensity variations along the CNT are identical in PEEM and SEM image and directly correlate with the topography of the CNT imaged with AFM.

Fig. 3a) shows an energy-filtered PEEM image at a binding energy E_B = 1.15 eV. The image was obtained as part of a sequence of images for which the retarding field analyzer was scanned from $E_{kin,S} + \phi_S = E_{kin,A} + \phi_A = h\nu - E_B = 2.45$ eV to 4.95 eV in steps of 50 meV. $E_{kin,S}$ is the kinetic energy of the electrons at the sample surface, $E_{kin,A}$ the kinetic energy at the analyzer, ϕ_S the work function of the sample, $\phi_A = 4.05$ eV the work function of the analyzer and $h\nu \approx 5$ eV the photon energy. The retarding field analyzer works as a high pass filter. For each cutoff setting only electrons with a kinetic energy higher than the cutoff can pass the filter. Every image was recorded for 10 seconds and a total of 80 scans are shown (FoV = 1.3 µm). Event counting was used to improve signal to noise ratio. The images were differentiated to obtain energy-filtered images. The energy scale has been corrected for sample charging resulting from photoemission of electrons. The charging effect has been estimated to be 0.1 eV by evaluation of the shift of the spectrum for different photon intensities. To correct this effect, the spectra have been shifted by 0.1 eV to lower binding energies.

The intensity located within the area enclosed by the white line (CNT) and the blue lines (SiC substrate) was determined for each resulting differential image and plotted as a function of E_B in Fig. 3b). We note that the resulting spectra are dominated by secondary electrons that superimpose the electronic structure of the CNT and substrate, respectively. Spectra were also determined for three different sections within the nanotube, with the aim to compare the markedly bright spot in the lower half of the tube with the rest. Sections and respective spectra are shown in Fig. S3. All spectra were found to be identical within the experimental uncertainties. This finding supports our conclusion that the bright spot on the CNT observed in the PEEM image is solely caused by topography. The spectra presented in Fig. 3b) and S3 clearly demonstrate the power of energy-filtered PEEM to image electronic structure on a nanometer scale.

The sample work function is given by the high binding energy cutoff of the spectra, which is obtained by numerically calculating the inflection point of the respective edge. This yields values of $\phi_{CNT} = 3.43 \pm 0.05$ eV for the CNT and $\phi_{SiC} = 3.08 \pm 0.05$ eV for the SiC substrate. The error corresponds to the energy interval of the measurement.

Furthermore, CNT and substrate show a distinct difference in the signal onset on the low binding energy side of the spectra resulting from their different electronic structure.

A comparison of our work function measurement with values reported in literature (ϕ_{SiC} = 4.3–4.89 eV [37–43], ϕ_{CNT} = 4.3–4.9 eV [44–48]) reveals significant deviations. However, when comparing our work function values to respective

literature values, several points have to be considered: (1) influence by the Schottky effect [49], (2) a contact potential between CNT and substrate, (3) doping of the CNT and (4) impact of contaminations. (1) The Schottky effect describes the influence of an electric field on the work function of materials. In the immersion lens of a PEEM, the sample itself is part of the objective lens, and thus exposed to an electric field perpendicular to the sample. In our experiment, this field is on the order of $E = 8\times10^6$ V/m. As an estimation, we treat the sample as a metal surface and obtain a lowering of the work function by $\Delta W = [e^3E / (4\pi\varepsilon_0)]^{1/2} = 0.11$ eV. Deviations due to the semiconducting nature of SiC and carbon nanotubes should be small [50]. The actual work functions are thus about 0.1 eV higher than the values obtained from Fig. 3b). (2) The work function difference of CNT and SiC substrate leads to a contact potential as the Fermi levels equilibrate. In our measurements, the CNT exhibits a higher work function than the SiC substrate. Accordingly, electrons flow from the SiC substrate onto the CNT. As a consequence of this charging and the resulting additional potential, the photoelectron spectrum of the CNT shifts to higher kinetic energies (lower binding energies), while the spectrum of the SiC substrate shifts to lower kinetic energies (higher binding energies). The actual work function difference of the CNT and SiC substrate should thus be smaller than measured. However, this effect cannot explain the deviation from literature values. (3) The investigated CNTs were grown with ammonia gas present, with the aim of nitrogen-doping. Nitrogen-doping is known to reduce the work function of CNTs. For capped (5,5) CNTs, Wen et al. computed that a substitutional nitrogen atom reduces the work function by about 0.5 eV [51]. (4) Furthermore, CNT and substrate are most likely contaminated with adsorbed water molecules and substances used during sample preparation (e.g. ethanol, salts). These adsorbates are likely to be the most dominant contribution to the difference between the literature values and our measurement of the work functions. In particular, adsorbed water is known to reduce the work function and ionization energy of carbon nanotubes [52]. We note that substrate spectra recorded on different locations on the sample are found to differ by not more than 0.1 eV (cf. Fig. S4b).

In summary, our results demonstrate the potential of energy-filtered PEEM to image differences in electronic structure on a nanometer scale. The deviation of obtained work function values from the literature values is mainly attributed to contaminations on the sample investigated here.

4. Conclusions

We have conducted UV-PEEM studies on multi-walled carbon nanotubes with unsurpassed spatial resolution. Complementary SEM and AFM measurements reveal that the intensity variations along the CNT originate from local field distortions due to topography of the nanotube. An imaging energy filter installed in the PEEM allowed us to obtain photoelectron spectra from a single CNT and even from several regions along the CNT. These spectra recorded along the CNT are identical within the experimental uncertainties, underlining that the PEEM contrast in this case is predominantly of topographic origin. With this, we shed light onto the importance of the different contrast mechanisms when imaging complex nano-objects with PEEM.

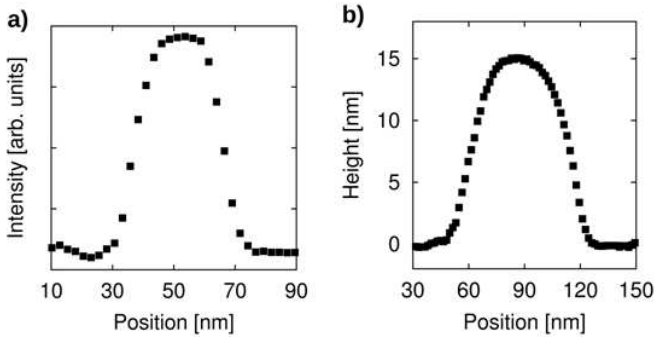

Figure S1. *a) Intensity profile of SEM measurement (FWHM = 29 nm) and b) height profile of AFM measurement (FWHM = 65 nm, height = 15 nm) along yellow lines in Fig. 3b) and c). In b) background has been subtracted.*

The work function determined from photoelectron spectra for the SiC substrate and the CNT is 0.9-1.8 eV lower than expected from literature. This is most likely due to adsorbates and residuals from sample preparation.

We conclude that photoemission electron microscopy (PEEM) has the potential to image complex nano-objects on surfaces with resolutions approaching those of a scanning electron microscope (SEM). In addition, energy-filtered PEEM bears great potential for fast imaging of electronic structure variation on nanometer length scales.

Acknowledgments

We thank Andrea Prager, Anika Gladytz, Ravikiran Chelur Suryaprakash and Dietmar Hirsch (Leibniz-Institute of Surface Modification) for SEM measurements. We are grateful for insightful discussion with Dietmar Hirsch (Leibniz-Institute of Surface Modification) and Martin Wolf (Fritz-Haber-Institute Berlin). We appreciate the support received from Dieter Polenz (FOCUS GmbH). CNT sample material was provided by Sossina M. Haile and Konstantinos P. Giapis (California Institute of Technology, Pasadena, USA). Nickel nanoparticles as CNT growth catalyst were provided by Nicholas Brunelli (Ohio State University). Andreas Neff was supported by a scholarship of the Beilstein-Institute, Germany. Katrin R. Siefermann was supported by the Robert-Bosch Foundation.

Appendix

SEM and AFM measurement

Fig. S1 shows line scans along the yellow lines shown in Fig. 2b) and c) of the SEM and AFM measurement. The size of the CNT in the AFM image differs considerably from PEEM (cf. line scan in Fig. 1c) and SEM images. While the CNT exhibits a height of about 15 nm, the FWHM has a value

of 65 nm. The height of the nanotube in the AFM measurement is roughly half as large as the width in the SEM measurement. This is most likely due to a deformation of the CNT by the AFM tip as the measurement was performed in tapping mode. Similar deformations of multi-walled CNTs during AFM measurements have been detected by Yu et. al. [53]. When increasing the force applied by the AFM tip, they observed a decrease of CNT height by almost one half, which is consistent with the ratio of the SEM width and AFM height of our measurement. We note, however, that the sample itself as well as the AFM settings used in [53] differ from our measurement. Furthermore, it is known that van der Waals interactions of CNTs with a substrate can lead to a deformation of the spherical structure even in absence of an AFM tip [54,55].

Another reason for the large ratio between the width and the height of the AFM measurement is the width of the tip itself, which is much larger than the CNT. Thus, one would expect to measure a larger width than height of a perfectly round nanotube.

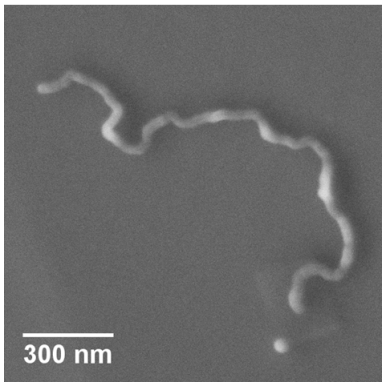

Figure S2. *SEM image of CNT at tilt of 30°. Combination of SE2 and InLens detector with ratio 1:1 (acceleration voltage: 3 kV).*

Fig. S2 shows an SEM image of the investigated CNT obtained at an acceleration voltage of 3 kV with a combination of SE2 and InLens detector signals at a ratio of 1:1. The sample was tilted by 30° to observe topography of the CNT.

Photoelectron Spectra

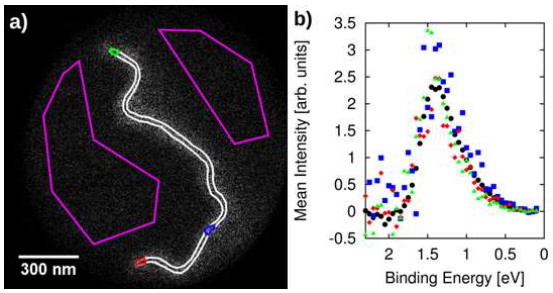

Figure S3. *a) Energy-filtered PEEM image at E_B = 1.15 eV. b) Photoelectron spectra of marked areas in a) (black circles: complete CNT, blue squares: bright spot in PEEM image, red diamonds: lower end of CNT, green triangles: upper end of CNT*

Fig. S3b) shows photoelectron spectra of several areas on the CNT together with the respective areas in a). As the selected areas are much smaller than the whole CNT, the noise in the spectra increases. Within the accuracy of the measurement, no change of the electronic valence structure can be observed for the bright spot in the PEEM image or the end of the CNT. This is in line with the AFM measurement indicating that the PEEM contrast is, in this case, topographic.

Fig. S4b) shows a comparison of photoelectron spectra of two different substrate areas of the same sample. The magenta area in Fig. S3a) exhibits a work function of 3.10 ± 0.05 eV while the white area in Fig. S4a) shows a work function of 3.18 ± 0.05 eV. We attribute the discrepancy to different concentrations of adsorbates and residual matter on the substrate.

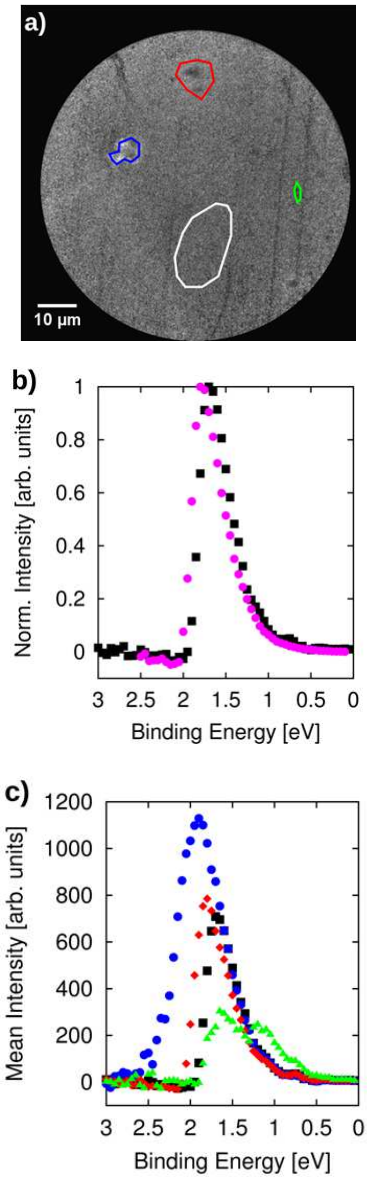

Figure S4. *a) Energy-filtered PEEM image at E_B = 1.8 eV. b) Comparison of two substrate areas. Magenta circles represent the spectrum for the respective area in Fig. S3a) and black squares for white area in Fig. S4a). c) Photoelectron spectra of respective areas indicated in a). Black squares represent spectrum for white area in a)*

Fig. S4c) shows photoelectron spectra of several areas marked in Fig. S4a). It reveals different electronic structure for different dirt particles on the substrate.

References

[1] A. Bailly, O. Renault, N. Barrett, L.F. Zagonel, P. Gentile, N. Pauc, et al., Direct quantification of gold along a single Si nanowire., Nano Lett. 8 (2008) 3709–3714.

[2] L. Douillard, F. Charra, Z. Korczak, R. Bachelot, S. Kostcheev, G. Lerondel, et al., Short range plasmon resonators probed by photoemission electron microscopy., Nano Lett. 8 (2008) 935–940.

[3] M. Hjort, J. Wallentin, R. Timm, a. a. Zakharov, J.N. Andersen, L. Samuelson, et al., Doping profile of InP nanowires directly imaged by photoemission electron microscopy, Appl. Phys. Lett. 99 (2011) 233113.

[4] S.J. Peppernick, A.G. Joly, K.M. Beck, W.P. Hess, Plasmonic field enhancement of individual nanoparticles by correlated scanning and photoemission electron microscopy., J. Chem. Phys. 134 (2011) 034507.

[5] L. Chelaru, M. Horn-von Hoegen, D. Thien, F.-J. Meyer zu Heringdorf, Fringe fields in nonlinear photoemission microscopy, Phys. Rev. B. 73 (2006) 115416.

[6] Y. Takamura, R. V Chopdekar, A. Scholl, A. Doran, J.A. Liddle, B. Harteneck, et al., Tuning magnetic domain structure in nanoscale La0.7Sr0.3MnO3 islands., Nano Lett. 6 (2006) 1287–1291.

[7] R. Könenkamp, R.C. Word, G.F. Rempfer, T. Dixon, L. Almaraz, T. Jones, 5.4 Nm Spatial Resolution in Biological Photoemission Electron Microscopy., Ultramicroscopy. 110 (2010) 899–902.

[8] R.C. Word, J.P.S. Fitzgerald, R. Könenkamp, Direct coupling of photonic modes and surface plasmon polaritons observed in 2-photon PEEM., Opt. Express. 21 (2013) 30507–30520.

[9] C. Lemke, T. Leißner, S. Jauernik, A. Klick, J. Fiutowski, J. Kjelstrup-Hansen, et al., Mapping surface plasmon polariton propagation via counter-propagating light pulses., Opt. Express. 20 (2012) 12877–12884.

[10] N.M. Buckanie, P. Kirschbaum, S. Sindermann, F.-J. Meyer zu Heringdorf, Interaction of light and surface plasmon polaritons in Ag islands studied by nonlinear photoemission microscopy., Ultramicroscopy. 130 (2013) 49–53.

[11] K. Fukumoto, K. Onda, Y. Yamada, T. Matsuki, T. Mukuta, S. Tanaka, et al., Femtosecond time-resolved photoemission electron microscopy for spatiotemporal imaging of photogenerated carrier dynamics in semiconductors., Rev. Sci. Instrum. 85 (2014) 083705.

[12] A Mikkelsen, J. Schwenke, T. Fordell, G. Luo, K. Klünder, E. Hilner, et al., Photoemission electron microscopy using extreme ultraviolet attosecond pulse trains., Rev. Sci. Instrum. 80 (2009) 123703.

[13] K. Siegrist, E.D. Williams, V.W. Ballarotto, Characterizing topography-induced contrast in photoelectron emission microscopy, J. Vac. Sci. Technol. A Vacuum, Surfaces, Film. 21 (2003) 1098.

[14] S.A. Nepijko, N.N. Sedov, C.H. Ziethen, G. Schönhense, M. Merkel, M. Escher, Peculiarities of imaging one- and two-dimensional structures in an emission electron microscope. 1. Theory, J. Microsc. 199 (2000) 124–129.

[15] S.A. Nepijko, N.N. Sedov, O. Schmidt, G. Schönhense, X. Bao, W. Huang, Imaging of three-dimensional objects in emission electron microscopy., J. Microsc. 202 (2001) 480–487.

[16] M. Lavayssière, M. Escher, O. Renault, D. Mariolle, N. Barrett, Electrical and physical topography in energy-filtered photoelectron emission microscopy of two-dimensional silicon pn junctions, J. Electron Spectros. Relat. Phenomena. 186 (2013) 30–38.

[17] V.K. Sangwan, V.W. Ballarotto, K. Siegrist, E.D. Williams, Characterizing voltage contrast in photoelectron emission microscopy., J. Microsc. 238 (2010) 210–217.

[18] S. Suzuki, Y. Watanabe, Y. Homma, S. Fukuba, S. Heun, A. Locatelli, Work functions of individual single-walled carbon nanotubes, Appl. Phys. Lett. 85 (2004) 127.

[19] S. Suzuki, Y. Watanabe, Y. Homma, S. Fukuba, A. Locatelli, S. Heun, Photoemission electron microscopy of individual single-walled carbon nanotubes, J. Electron Spectros. Relat. Phenomena. 144-147 (2005) 357–360.

[20] V.K. Sangwan, Carbon Nanotube Thin Film as an Electronic Material, PhD thesis, University of Maryland, 2009.

[21] D. Deng, L. Yu, X. Chen, G. Wang, L. Jin, X. Pan, et al., Iron encapsulated within pod-like carbon nanotubes for oxygen reduction reaction., Angew. Chemie. 52 (2013) 371–375.

[22] R.H. Baughman, A.A. Zakhidov, W.A. de Heer, Carbon nanotubes--the route toward applications., Science (80-.). 297 (2002) 787–792.

[23] W. Yang, P. Thordarson, J.J. Gooding, S.P. Ringer, F. Braet, Carbon nanotubes for biological and biomedical applications, Nanotechnology. 18 (2007) 412001.

[24] V. Popov, Carbon nanotubes: properties and application, Mater. Sci. Eng. R Reports. 43 (2004) 61–102.

[25] S. Suzuki, C. Bower, Y. Watanabe, O. Zhou, Work functions and valence band states of pristine and Cs-intercalated single-walled carbon nanotube bundles, Appl. Phys. Lett. 76 (2000) 4007.

[26] S. Suzuki, Y. Watanabe, S. Heun, Photoelectron spectroscopy and microscopy of carbon nanotubes, Curr. Opin. Solid State Mater. Sci. 10 (2006) 53–59.

[27] J.W. Chiou, C.L. Yueh, J.C. Jan, H.M. Tsai, W.F. Pong, I.-H. Hong, et al., Electronic structure of the carbon nanotube tips studied by x-ray-absorption spectroscopy and scanning photoelectron microscopy, Appl. Phys. Lett. 81 (2002) 4189.

[28] S. Suzuki, Y. Watanabe, T. Kiyokura, K. Nath, T. Ogino, S. Heun, et al., Electronic structure at carbon nanotube tips studied by photoemission spectroscopy, Phys. Rev. B. 63 (2001) 245418.

[29] S. Suzuki, Y. Watanabe, T. Ogino, S. Heun, L. Gregoratti, a. Barinov, et al., Electronic structure of carbon nanotubes studied by photoelectron spectromicroscopy, Phys. Rev. B. 66 (2002) 035414.

[30] W. Li, Y. Zhou, H.-J. Fitting, W. Bauhofer, Imaging mechanism of carbon nanotubes on insulating and conductive substrates using a scanning electron microscope, J. Mater. Sci. 46 (2011) 7626–7632.

[31] Y. Homma, S. Suzuki, Y. Kobayashi, M. Nagase, D. Takagi, Mechanism of bright selective imaging of single-walled carbon nanotubes on insulators by scanning electron microscopy, Appl. Phys. Lett. 84 (2004) 1750.

[32] Á. Varga, M. Pfohl, N. a Brunelli, M. Schreier, K.P. Giapis, S.M. Haile, Carbon nanotubes as electronic interconnects in solid acid fuel cell electrodes., Phys. Chem. Chem. Phys. 15 (2013) 15470–15476.

[33] J. Lin, N. Weber, A. Wirth, S.H. Chew, M. Escher, M. Merkel, et al., Time of flight-photoemission electron microscope for ultrahigh spatiotemporal probing of nanoplasmonic optical fields., J. Phys. Condens. Matter. 21 (2009) 314005.

[34] C. Ziethen, O. Schmidt, G.H. Fecher, C.M. Schneider, G. Schönhense, R. Frömter, et al., Fast elemental mapping and magnetic imaging with high lateral resolution using a novel photoemission microscope, J. Electron Spectros. Relat. Phenomena. 88-91 (1998) 983–989.

[35] S.A. Nepijko, N.N. Sedov, Resolution deterioration in emission and electron microscopy due to object roughness, Ann. Phys. 9 (2000) 441–451.

[36] J. Stöhr, S. Anders, X-ray spectro-microscopy of complex materials and surfaces, IBM J. Res. Dev. 44 (2000) 535–551.

[37] M. Wiets, M. Weinelt, T. Fauster, Electronic structure of SiC(0001) surfaces studied by two-photon photoemission, Phys. Rev. B. 68 (2003) 125321.

[38] V. Van Elsbergen, T. Kampen, W. Mönch, Surface analysis of 6H-SiC, Surf. Sci. 365 (1996) 443–452.

[39] T. Jikimoto, J.L. Wang, T. Saito, M. Hirai, M. Kusaka, M. Iwami, et al., Atomic and electronic structures of heat treated 6H–SiC surface, Appl. Surf. Sci. 130-132 (1998) 593–597.

[40] S. Kennou, An x-ray photoelectron spectroscopy and work-function study of the Er/α-SiC(0001) interface, J. Appl. Phys. 78 (1995) 587.

[41] S. Kennou, A. Siokou, I. Dontas, S. Ladas, An interface study of vapor-deposited rhenium with the two (0001) polar faces of single crystal 6H-SiC, Diam. Relat. Mater. 6 (1997) 1424–1427.

[42] J. Pelletier, D. Gervais, C. Pomot, Application of wide-gap semiconductors to surface ionization: Work functions of AlN and SiC single crystals, J. Appl. Phys. 55 (1984) 994.

[43] C. Benesch, M. Fartmann, H. Merz, k-resolved inverse photoemission of four different 6H-SiC (0001) surfaces, Phys. Rev. B. 64 (2001) 205314.

[44] Z. Xu, X.D. Bai, E.G. Wang, Z.L. Wang, Field emission of individual carbon nanotube with in situ tip image and real work function, Appl. Phys. Lett. 87 (2005) 163106.

[45] R. Gao, Z. Pan, Z.L. Wang, Work function at the tips of multiwalled carbon nanotubes, Appl. Phys. Lett. 78 (2001) 1757.

[46] P. Liu, Q. Sun, F. Zhu, K. Liu, K. Jiang, L. Liu, et al., Measuring the work function of carbon nanotubes with thermionic method., Nano Lett. 8 (2008) 647–651.

[47] H. Ago, T. Kugler, F. Cacialli, W.R. Salaneck, M.S.P. Shaffer, A.H. Windle, et al., Work Functions and Surface Functional Groups of Multiwall Carbon Nanotubes, J. Phys. Chem. B. 103 (1999) 8116–8121.

[48] M. Shiraishi, M. Ata, Work function of carbon nanotubes, Carbon N. Y. 39 (2001) 1913–1917.

[49] W. Schottky, Influence of structure-action, especially the Thomson constructive force, on the electron emission of metals, Phys. Zeitschrift. 15 (1914).

[50] G. Busch, J. Wullschleger, Der Schottky-Effekt an reinen Silizium-Oberflächen, Phys. Der Kondens. Mater. 12 (1970) 47–71.

[51] Q.B. Wen, L. Qiao, W.T. Zheng, Y. Zeng, C.Q. Qu, S.S. Yu, et al., Theoretical investigation on different effects of nitrogen and boron substitutional impurities on the structures and field emission properties for carbon nanotubes, Phys. E Low-Dimensional Syst. Nanostructures. 40 (2008) 890–893.

[52] C. Kim, Y.S. Choi, S.M. Lee, J.T. Park, B. Kim, Y.H. Lee, The Effect of Gas Adsorption on the Field Emission Mechanism of Carbon Nanotubes, J. Am. Chem. Soc. 124 (2002) 9906–9911.

[53] M. Yu, T. Kowalewski, R. Ruoff, Investigation of the radial deformability of individual carbon nanotubes under controlled indentation force, Phys. Rev. Lett. 85 (2000) 1456–1459.

[54] T. Hertel, R. Walkup, P. Avouris, Deformation of carbon nanotubes by surface van der Waals forces, Phys. Rev. B. 58 (1998) 13870–13873.

[55] R.S. Ruoff, J. Tersoff, D.C. Lorents, S. Subramoney, B. Chan, Radial deformation of carbon nanotubes by van der Waals forces, Nature. 364 (1993) 514–516.